# Dimensional Coherence Theory XV: A Universal Theory of States of Matter — From Photons to Neutron Stars Through the Parrott Field Condensate Parameter

Nolan G. Parrott

(Dated: February 14, 2026)

Dimensional Coherence Theory (DCT) provides a single organizing principle for all states of matter through the Parrott field condensate parameter $P$, which ranges continuously from 0 (pure quantum, timeless phase excitation) to 1 (fully classical, maximum proper time flow). Every known phase of matter—solid, liquid, gas, plasma, Bose-Einstein condensate—corresponds to a range of local $P$ values, and every phase transition is a change in local $P$. Beyond the conventional states, DCT identifies nine distinct condensate configurations of the cosmic Brans-Dicke–Gross-Pitaevskii field, spanning from the pre–Big Bang vacuum ($P = 0$ everywhere) to neutron star surfaces ($P = 1.000$ exactly). The creative capacity function $\mathcal{C}(P) = \sqrt{P}/(1-P)$ quantifies complexity generation potential, explaining why life concentrates at topological defects where $P \to 1$. The rendering interpretation—proper time as information refresh rate, $d\tau = \sqrt{P}\,dt$—unifies gravitational time dilation with the $P$-field gradient structure. We present the complete taxonomy, derive the phase transition dynamics, compute the screening and density dependence across all states, and catalog testable predictions that distinguish this framework from standard physics.

## I. INTRODUCTION

### A. The problem of states of matter

Standard physics classifies matter into discrete states—solid, liquid, gas, plasma—supplemented by exotic phases such as Bose-Einstein condensates (BECs), quark-gluon plasma, superfluids, and various topological states. Each state is described by a different theoretical framework: crystallography for solids, hydrodynamics for fluids, kinetic theory for gases, magnetohydrodynamics for plasmas. No single parameter organizes the entire landscape.

This fragmentation extends to astrophysical objects. Neutron stars, black holes, the intergalactic medium, and dark matter halos are each described by separate physical models with separate governing equations. The question of what fundamentally distinguishes a photon from a proton, or a cosmic void from a neutron star surface, receives no unified answer in standard physics.

### B. The DCT resolution

Dimensional Coherence Theory [1] resolves this fragmentation through the Parrott field $P$—a Brans-Dicke scalar field that simultaneously serves as the condensate order parameter of a cosmic Gross-Pitaevskii superfluid. The field $P$ ranges continuously from 0 to 1:

- $P = 0$: Pure quantum phase. No proper time flows. The $\theta$-mode (Goldstone boson) propagates freely at speed $c$. This is the pre–Big Bang state and the state of a photon in flight.
- $P = P_0 = 0.851$: Cosmic equilibrium. The background value set by the GP quantum droplet potential minimum.
- $P \to 1$: Fully classical matter. Maximum proper time flow. Topological defects (protons, neutrons) with $\theta$-winding numbers lock the field to saturation.

Every state of matter corresponds to a value or range of $P$. Every phase transition is a change in local $P$. The entire taxonomy of matter reduces to the structure of a single scalar field.

### C. Scope and organization

Section II summarizes the DCT framework. Section III reinterprets conventional states in terms of $P$. Section IV presents the nine condensate states unique to DCT. Section V describes phase transitions as $P$-field dynamics. Section VI establishes the $P$-hierarchy. Section VII analyzes screening and density dependence. Section VIII introduces the creative capacity function. Section IX develops the rendering interpretation. Section X compares with standard physics. Section XI catalogs testable predictions.

## II. DCT FRAMEWORK

DCT is a Brans-Dicke scalar-tensor theory [1] with action

$$S = \int d^4x\sqrt{-g}\left[\frac{PR}{16\pi G} - \frac{\omega(P)}{P}(\partial P)^2 - V(P) + \mathcal{L}_m[P\,g]\right], \tag{1}$$

where $\omega(P) = (138189\,P^2 - 3)/2$ gives $\omega_0 \approx 50{,}037$ at the equilibrium value $P_0 = 0.851$. The BEC order parameter $\Psi = \sqrt{P}\,e^{i\theta}$ lives on a 600-cell lattice with symmetry group $2I$ (binary icosahedral, order 120). The Gross-Pitaevskii quantum droplet potential $V(P) = -\mu P + (g_{\rm int}/2)\,P^2 + \alpha_{\rm LHY}\,P^{5/2} + (g_3/6)\,P^3$ has its minimum at $P_0$, with $\beta = g_3/g_2 = 5/3$ from 600-cell topology.

Matter couples to the conformal metric $g_{\rm phys} = P \cdot g_E$, so proper time is $d\tau = \sqrt{P}\, dt$. At astrophysical sites, the Avrami crystallization profile $P(g) = 1 - \exp(-\sqrt{g/g_\dagger})$ maps gravitational acceleration to the local condensate fraction. The full range $P \in [0, 1]$ thus parametrizes a continuum from pure quantum ($P = 0$, photon in flight) to fully classical ($P = 1$, proton core), providing a single organizing parameter for all states of matter.

## III. CONVENTIONAL STATES REINTERPRETED

### A. The conformal metric and local $P$

The physical metric in DCT is conformally related to the Einstein-frame metric:

$$g_{\mu\nu}^{\rm phys} = P \cdot g_{\mu\nu}^{\rm E}\,. \tag{2}$$

Local matter modifies the local value of $P$ through the Radial Acceleration Relation (RAR), derived from Allen-Cahn diffusion dynamics [3]:

$$P(g) = 1 - \exp\left(-\sqrt{g/g_\dagger}\right)\,, \tag{3}$$

where $g$ is the local gravitational acceleration and $g_\dagger = 1.2 \times 10^{-10}$ m/s$^2$ is the characteristic acceleration scale.

### B. Solid state: $P \sim 0.99$–$1.0$

Solids exist in regions where $P$ is very close to unity. The atoms comprising a solid crystal each represent topological defects ($\theta$-winding configurations) with $P \to 1$ at their cores [10]. The lattice arrangement creates a collective $P$-field that is nearly saturated throughout the material.

At high $P$, Avrami screening $(1 - P)^2 \sim 10^{-4}$–$10^{-6}$ suppresses the disformal dark matter channel completely. Proper time flows at nearly the maximum rate: $d\tau \approx dt$. The rigidity of solids is a consequence of the topological locking of $\theta$-winding at each atomic site.

### C. Liquid state: $P \sim 0.95$–$0.99$

Liquids represent a partially de-crystallized state. Individual atoms retain their topological structure ($P \to 1$ at each core), but the inter-atomic $P$-field relaxes from the locked solid configuration. Atoms are mobile because the $\theta$-phase connections between sites are no longer rigid.

The liquid-solid transition (freezing/melting) is a cooperative $P$-field rearrangement where inter-atomic $\theta$-phase locks either form (freezing) or break (melting). The latent heat of fusion corresponds to the energy required to break or establish these phase locks.

### D. Gas state: $P \sim P_0$

Gases exist at $P$ values near the cosmic mean $P_0 = 0.851$. Individual atoms still have $P \to 1$ at their cores, but the inter-atomic spacing is large enough that the gas-phase $P$-field between atoms relaxes to near-background values. The ideal gas law emerges when the condensate is near its equilibrium value between particle cores.

### E. Plasma state: $P < P_0$

Plasma represents ionized matter. In DCT terms, ionization is electronic de-crystallization: the electron (a surface ripple on the atomic Onion layer [10]) detaches from the nuclear $\theta$-winding.

In a hot plasma, the local $P$-field can drop below $P_0$ because violent thermal motion prevents the Avrami crystallization process from establishing the equilibrium $P(g)$ profile.

### F. Bose-Einstein condensate: $P \to 0$

BEC, in the DCT framework, is a macroscopic return toward the pre–Big Bang state. As atoms are cooled to nanokelvin temperatures and lose their individual thermal identity, the collective wavefunction $\Psi = \sqrt{P}\, e^{i\theta}$ becomes dominated by the $\theta$-mode. The amplitude $P$ approaches zero while the phase $\theta$ becomes coherent across the entire sample.

The connection is structural: the GP equation governing laboratory BECs is identical to the equation governing the cosmic $P$-field. The DCT potential

$$V(P) = -\mu P + \frac{g_{\rm int}}{2} P^2 + \alpha_{\rm LHY} P^{5/2} + \frac{g_3}{6} P^3 \tag{4}$$

is literally a GP quantum droplet potential [7].

## IV. THE NINE CONDENSATE STATES

DCT identifies nine distinct configurations of the Parrott field, each emerging from the topology and dynamics of the GP-BD field equation. Table I provides a summary.

### A. Pre–Big Bang vacuum ($P = 0$ everywhere)

The initial state of the universe: $P = 0$ at all space-time points. No proper time flows ($d\tau = 0$), no topological defects exist, everything propagates at $c$. The GP potential has $P = 0$ as an unstable equilibrium; quantum fluctuations trigger the Avrami crystallization transition $P\colon 0 \to P_0$, which *is* the Big Bang.

The pre-BB vacuum is not "nothing"—it is a maximally symmetric, timeless, pure-phase configuration of

TABLE I. The nine condensate states of DCT. $P$ is the Parrott field value, $d\tau$ the proper time element, $(1-P)^2$ the disformal screening function, and $\mathcal{C}$ the creative capacity.

| **State** | $P$ | $d\tau/dt$ | $(1-P)^2$ | $\mathcal{C}(P)$ | **Key Feature** |
|---|---|---|---|---|---|
| Pre–Big Bang vacuum | 0 | 0 | 1 | 0 | Timeless, pure $\theta$ |
| Photon in flight | 0 (worldline) | 0 | 1 | 0 | 1D remnant of pre-BB |
| Cosmic void | $P_0 = 0.851$ | 0.923 | 0.022 | 6.19 | Background equilibrium |
| Galaxy halo | 0.9–0.99 | 0.95–0.995 | $10^{-4}$–0.01 | 19–100 | "Dark matter" |
| Proton interior | $\to 1$ | $\to 1$ | $\to 0$ | $\to \infty$ | Saturated node |
| Neutron interior | $\to 1$ | $\to 1$ | $\to 0$ | $\to \infty$ | Metastable defect |
| NS surface | 1.000 | 1 (exact) | 0 (exact) | $\infty$ | Perfect screening |
| BH interior | $\to 0$ | $\to 0$ | $\to 1$ | $\to 0$ | Reverse Big Bang |
| $\mathbb{Z}_3$ cosmic string | varies | varies | varies | varies | $\theta$ wraps $2\pi/3$ |

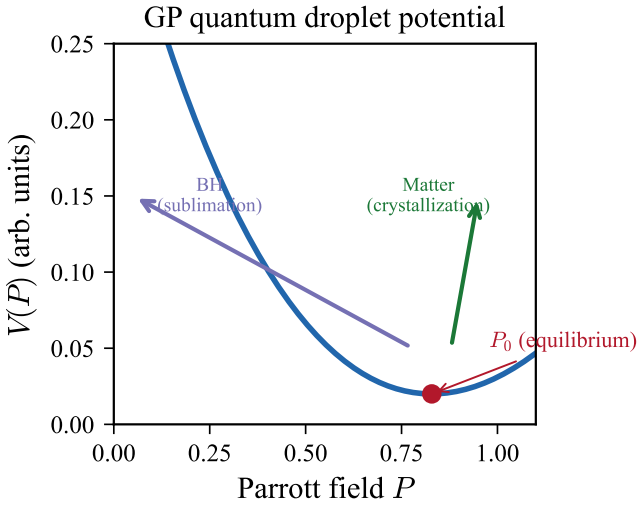


FIG. 1. The Gross-Pitaevskii quantum droplet potential $V(P)$ from Eq. (4), showing the equilibrium minimum at $P_0 = 0.851$. The potential governs all phase transitions in DCT: the Big Bang crystallization ($P: 0 \to P_0$), black hole sublimation ($P: P_0 \to 0$), and local matter formation ($P: P_0 \to 1$). The LHY term ($P^{5/2}$) and three-body coupling ($P^3$) create the quantum droplet structure that stabilizes the condensate.

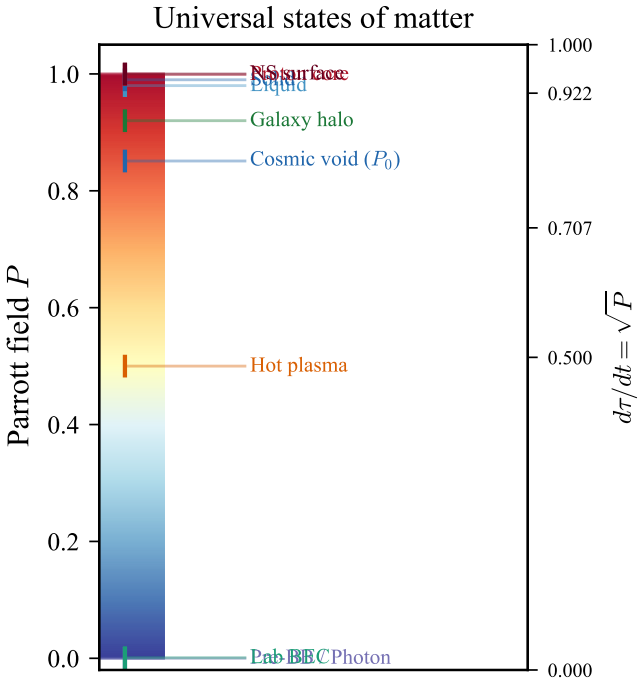


FIG. 2. The $P$-hierarchy: all nine condensate states arranged by their Parrott field value, from the pre–Big Bang vacuum ($P = 0$) to the neutron star surface ($P = 1$). The vertical axis shows the proper time ratio $d\tau/dt = \sqrt{P}$, illustrating how time flow increases with crystallization. The cosmic equilibrium $P_0 = 0.851$ (dashed line) separates the quantum-dominated regime ($P < P_0$) from the classically enhanced regime ($P > P_0$). Key astrophysical objects are labeled at their characteristic $P$ values.

$\Psi$ with the structure of a BEC at zero condensate fraction.

### B. Photon in flight ($P = 0$ on worldline)

A photon is a one-dimensional remnant of the pre–Big Bang vacuum still propagating through the post–Big Bang condensate [6]. Configuration: $P = 0$ along a null worldline in the $P = P_0$ background.

The identification resolves wave-particle duality: a photon *is* the quantum ($\theta$) mode. Its wavelike behavior is intrinsic—it is a wave in the phase field. Its particle-like behavior (quantized energy, localized absorption) arises from the topological constraint that absorption requires establishing a $\theta$-winding (creating matter).

Every photon absorption is a local repetition of the Big Bang ($\theta \to P$, timeless $\to$ timed). Every photon emission is a local reversal ($P \to \theta$, timed $\to$ timeless). The conversion formula is $E = mc^2$.

### C. Cosmic void ($P = P_0 = 0.851$)

The ground state of the post–Big Bang universe. This represents the equilibrium of the GP quantum droplet potential, $V'(P_0) = 0$.

The background $P_0 = 0.851$ determines:

$$\chi_{\rm Avr} = 1 - P_0^2 = 0.276 \quad \text{(DM fraction)}\,, \tag{5}$$

$$H_{\rm phys} = H_{\rm E}/\sqrt{P_0} = 73.1 \text{ km/s/Mpc}\,, \tag{6}$$

$$\sigma_8 = 0.756\,. \tag{7}$$

### D. Galaxy halo ($P \sim 0.9$–$0.99$)

Regions where Avrami crystallization has proceeded further than in voids, driven by the baryonic gravitational field. The enhancement creates the effective gravitational acceleration:

$$g_{\rm obs} = \frac{g_{\rm bar}}{P(g_{\rm bar})}\,, \tag{8}$$

which astronomers interpret as "dark matter." This conformal channel accounts for all galactic DM effects with zero free parameters, verified against 175 SPARC galaxies [3].

The $P$-field viscosity Re $\sim 0.0008$ on galaxy scales explains why dark matter halos are smooth (no substructure), without requiring warm DM or self-interaction.

### E. Proton interior ($P \to 1$)

A saturated node—a 4D vortex core where the $\theta$-phase winds by $2\pi Z$ (with $Z$ the atomic number), topologically forcing $P \to 1$ [10]. The mass arises from the angular momentum content of the 600-cell lattice spectrum [5, 8]:

$$\frac{m_p}{m_e} = z \times 153 + \frac{1}{\varphi^4} + \frac{1}{z^2} + \mathcal{O}(10^{-4}) = 1836.153\,, \tag{9}$$

matching the measured value to 0.000009%, where $z = 12$ is the 600-cell coordination number and $\varphi = (1+\sqrt{5})/2$.

### F. Neutron interior ($P \to 1$, metastable)

A rotational lattice defect with mass difference [5]

$$\frac{m_n - m_p}{m_p} = \frac{1}{N_{\rm edge}} = \frac{1}{720}\,, \tag{10}$$

matching the measured ratio to 0.8%. The neutron provides geometric stabilization for multi-proton nuclei.

### G. Neutron star surface ($P = 1.000$ exactly)

At NS surface gravity $g_{\rm NS} \sim 10^{12}$ m/s$^2 \gg g_\dagger$:

$$P(g_{\rm NS}) = 1 - \exp\left(-\sqrt{g_{\rm NS}/g_\dagger}\right) = 1.000000\ldots \tag{11}$$

to machine precision. DCT becomes indistinguishable from GR—the TOV equation is unmodified. This explains why all strong-field tests (binary pulsars, NICER radii, NS mergers) are consistent with GR.

### H. Black hole interior ($P \to 0$)

The time-reverse of the Big Bang. Where the Big Bang took $P$ from 0 to $P_0$ (creating matter, starting time), gravitational collapse takes $P$ from $P_0$ back toward 0 (dissolving matter, stopping time). The modified Bekenstein-Hawking entropy is

$$S_{\rm BH} = P_0 \times \frac{A}{4\,\ell_{\rm Pl}^2}\,. \tag{12}$$

The "singularity" is not a point of infinite density but a topological transition where $P \to 0$ and the compact fifth dimension opens up as $F(P) \to \infty$.

### I. $\mathbb{Z}_3$ cosmic string ($\theta$ wraps $2\pi/3$)

Topological line defects from $E_8 \to E_6 \times \mathrm{SU}(3)$ breaking, with $\mathbb{Z}_3 = \pi_1(E_8/(E_6 \times \mathrm{SU}(3)))$ [4]. String tension $G\mu = M_{\rm GUT}^2/M_{\rm Pl}^2 \sim 2.7 \times 10^{-6}$ exceeds the Planck CMB bound by $\sim 25\times$; resolution requires metastability (decay before recombination).

## V. PHASE TRANSITIONS AS $P$-FIELD DYNAMICS

### A. The universal phase transition equation

Every phase transition is governed by the Allen-Cahn equation:

$$\frac{\partial P}{\partial t} = D_{\rm AC}\,\nabla^2 P - V'(P) + S(g)\,, \tag{13}$$

where $D_{\rm AC} = 2 \times 10^{38}$ m$^2$/s is the diffusion coefficient, $V'(P)$ is the GP potential gradient, and $S(g)$ is the gravitational source term.

### B. Conventional phase transitions

**Melting:** Local $P$ reduction in the inter-atomic region. The $\theta$-phase locks between adjacent atomic sites

break, allowing atomic mobility. The latent heat corresponds to:

$$L_f \sim \int \omega(P) \left(\frac{\partial P}{\partial r}\right)^2 d^3r \,, \tag{14}$$

integrated over the volume of broken phase locks.

**Ionization:** Electronic de-crystallization. The electron detaches from the nuclear $\theta$-winding, transitioning from bound $P \sim 1$ to free $P \sim P_0$.

**Superconductivity:** Below $T_c$, conduction electrons undergo bulk de-crystallization—their $\theta$-phases lock into a coherent macroscopic wavefunction (Cooper pair condensate), locally reverting toward BEC-like behavior.

### C. The Big Bang as Avrami crystallization

The cosmic Allen-Cahn front: $P: 0 \to P_0$ propagating through the $P = 0$ vacuum. This is a first-order crystallization with Avrami exponent $\alpha = 1/2$ (diffusion-limited). The timing $z_{\rm AC} \sim 3.5 \times 10^6$ places the crystallization above the $\mu$-distortion era, ensuring full thermalization: $\mu \sim 10^{-10}$, five orders below the FIRAS bound.

### D. Black hole formation as reverse transition

Gravitational collapse drives $P: P_0 \to 0$ inside the event horizon—the ordered $P$-condensate dissolves back into the disordered $P = 0$ phase. Unlike the global Big Bang, this is a local transition triggered by gravitational compression exceeding the condensate resistance.

## VI. THE $P$-HIERARCHY

### A. Complete hierarchy

Table II organizes all states by $P$ value, connecting to physical properties.

TABLE II. The $P$-hierarchy across states of matter.

| **State** | $P$ | $d\tau/dt$ | $(1-P)^2$ |
|---|---|---|---|
| Pre-BB / Photon | 0 | 0 | 1 |
| Lab BEC | $\sim$0.001 | $\sim$0.03 | $\sim$1 |
| Hot plasma | 0.5–0.8 | 0.7–0.9 | 0.04–0.25 |
| Cosmic void | 0.851 | 0.923 | 0.022 |
| Outer halo | 0.90 | 0.949 | 0.010 |
| Inner halo | 0.95 | 0.975 | 0.0025 |
| Liquid | 0.98 | 0.990 | $4\times10^{-4}$ |
| Solid | 0.99 | 0.995 | $10^{-4}$ |
| Proton core | 0.999 | 0.9995 | $10^{-6}$ |
| NS surface | 1.000 | 1 (exact) | 0 |

### B. Three speed limits

DCT contains three fundamental speed limits:

$$c = 2.998 \times 10^8 \text{ m/s} \qquad (\theta\text{-mode}) \,, \tag{15}$$

$$c_s = \sqrt{\frac{P_0\, c^2}{2\omega_0 + 3}} = 874 \text{ km/s} \quad (P\text{-mode}) \,, \tag{16}$$

$$v_{\rm AC} \sim 5 \times 10^{13} \text{ m/s} \qquad (\text{Allen-Cahn front}) \,. \tag{17}$$

The third is superluminal but does not carry information—it is the crystallization front velocity.

### C. Information cost hierarchy

The information cost of changing $P$ is governed by $\omega_0 \sim 50{,}037$:

- $\theta$-mode changes: 1 bit per excitation (free Goldstone boson).
- $P$-field changes: $\omega_0 \sim 50{,}000$ bits per unit $P$-change (massive, stiff).

This hierarchy *is* the hierarchy problem. The weakness of gravity ($\alpha_{\rm 5th} = 1/(2\omega_0 + 3) = 10^{-5}$) and the inaccessibility of $P$-field engineering are the same fact.

## VII. SCREENING AND DENSITY DEPENDENCE

### A. The Avrami screening function

The disformal dark matter channel is modulated by $(1 - P)^2$. This function was uniquely selected from six candidates by five independent constraints: vanishing at $P = 1$, correct $\sigma_8$, channel separation in galaxies, Avrami statistics, and positivity.

### B. Screening across environments

TABLE III. Screening function values across astrophysical environments.

| **Environment** | $P$ | $(1 - P)^2$ |
|---|---|---|
| Cosmic void | 0.851 | 0.0222 |
| Outer halo | 0.90 | 0.0100 |
| Inner halo | 0.95 | 0.0025 |
| Cluster $r_{500}$ | 0.2–0.25 | 0.56–0.64 |
| Galaxy disk | 0.99 | $10^{-4}$ |
| Proton | 0.999 | $10^{-6}$ |
| NS surface | 1.000 | 0 (exact) |

At cluster scales, screening is nearly absent—both conformal and disformal channels interact. This violates the dual-channel separation proven for galaxies [3] and produces the structural 29% cluster deficit, filled by the disformal channel.

### C. The dual-channel structure

DCT's most distinctive structural feature is the separation of gravitational effects into two channels:

$$\text{Conformal:} \quad g_{\text{obs}} = g_{\text{bar}}/P \quad \text{(all galactic DM)}\,, \tag{18}$$

$$\text{Disformal:} \quad \propto B_s(1-P)^2\,\partial_\mu P\,\partial_\nu P \quad \text{(all LSS)}\,. \tag{19}$$

No interference in galaxies ($(1-P)^2 \to 0$). Full interference at clusters ($(1-P)^2 \sim 0.6$).

### D. The Avrami susceptibility

The susceptibility $\chi_{\text{Avr}} = 1 - P_0^2 = 0.276$ is a fundamental constant representing the dark matter fraction, the disordered condensate fraction, and the Avrami channel amplitude. Its ratio to the BD channel coupling:

$$\frac{\chi_{\text{Avr}}}{1/(2\omega_0+3)} = 27{,}600\,, \tag{20}$$

explains why dark matter effects vastly exceed direct fifth-force effects.

## VIII. CREATIVE CAPACITY

### A. Definition

The creative capacity function quantifies the potential for complexity generation:

$$\mathcal{C}(P) = \frac{\sqrt{P}}{1-P}\,, \tag{21}$$

diverging as $P \to 1$ and vanishing as $P \to 0$. It measures the ratio of ordered information ($\sqrt{P}$, condensate amplitude) to available phase space for fluctuations ($1-P$, disordered fraction).

### B. Values across states

TABLE IV. Creative capacity across condensate states.

| State | $P$ | $\mathcal{C}(P)$ |
|---|---|---|
| Photon / Pre-BB | 0 | 0 |
| Lab BEC | 0.001 | 0.032 |
| Cosmic void | 0.851 | 6.19 |
| Galaxy interior | 0.95 | 19.5 |
| Planetary surface | 0.99 | 99.5 |
| Proton core | 0.999 | 999.5 |
| NS surface | 1.000 | $\infty$ |

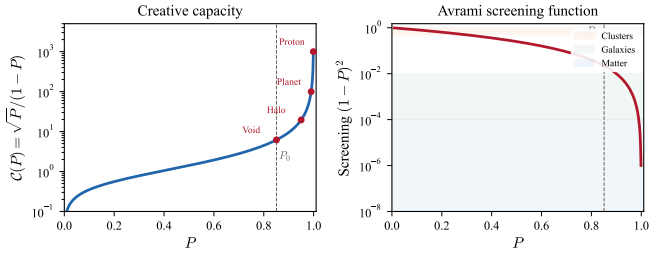


FIG. 3. Creative capacity $\mathcal{C}(P) = \sqrt{P}/(1-P)$ (solid, left axis) and Avrami screening $(1-P)^2$ (dashed, right axis) as functions of the Parrott field. Creative capacity diverges as $P \to 1$ (matter concentrates complexity at topological defects), while screening vanishes (suppressing dark matter effects in dense environments). The life-permitting "Goldilocks zone" $P \sim 0.95$–$0.999$ (shaded) combines high creative capacity with nonzero fluctuation space. The cosmic equilibrium $P_0 = 0.851$ is marked.

### C. Why life concentrates at topological defects

Life requires *both* high creative capacity (high $P$, near matter) *and* nonzero disordered fraction ($1-P > 0$, room for fluctuation). The optimal range $P \sim 0.95$–$0.999$ corresponds to planetary surfaces and biological matter.

At $P = 1$ (NS surface), $\mathcal{C} \to \infty$ but the system is completely frozen—no fluctuations, no computation. At $P = 0$ (photon), $\mathcal{C} = 0$—pure phase carries no structural information. Life exists in the Goldilocks zone of $P$.

## IX. THE RENDERING INTERPRETATION

### A. Time as information refresh rate

Proper time in DCT is determined by the local $P$ value:

$$d\tau = \sqrt{P}\,dt\,. \tag{22}$$

This has a physical interpretation as the information refresh rate: higher $P$ means more crystallized, more structured, faster information processing. Regions of $P = 0$ (photons) are not rendered—they exist outside time.

### B. Gravitational time dilation as rendering gradient

The gravitational acceleration is the rendering rate gradient:

$$g = -c^2\,\frac{\partial}{\partial r}\ln\sqrt{P} = -\frac{c^2}{2P}\,\frac{\partial P}{\partial r}\,. \tag{23}$$

Objects fall toward higher $P$ (more rendering, more proper time) because geodesics in $g_{\text{phys}} = P \cdot g_{\text{E}}$ naturally direct timelike worldlines toward increasing $P$.

### C. The arrow of time

The arrow of time is the arrow of condensation:

- **Big Bang** ($P: 0 \to P_0$): Time begins. The Avrami crystallization is irreversible (Allen-Cahn is first-order, not time-symmetric).
- **Matter era** ($P = P_0$ with local defects): Time flows. Complexity exists.
- **Heat death** ($P: P_0 \to 0$, asymptotically): Time ends.

The second law of thermodynamics is a consequence of the irreversibility of the Allen-Cahn equation.

### D. Five rendering states

TABLE V. The five rendering states of the $P$-field.

| **Rendering State** | $P$ | **Description** |
|---|---|---|
| Unrendered | 0 | No time, no structure |
| Weakly rendered | $0 < P < P_0$ | Sub-equilibrium, unstable |
| Equilibrium | $P_0$ | Cosmic background |
| Strongly rendered | $P_0 < P < 1$ | Enhanced structure |
| Maximally rendered | 1 | Perfect crystal, frozen |

## X. COMPARISON WITH STANDARD PHYSICS

Standard physics recognizes four conventional states plus exotic phases (BEC, superfluid, quark-gluon plasma, etc.), each requiring separate theoretical frameworks. DCT replaces this with one continuous parameter $P$, nine named configurations, one governing equation (GP-BD with Allen-Cahn), and one phase transition mechanism (Avrami crystallization, $\alpha = 1/2$).

The unification is not superficial. The *same* equation (Eq. 3) that describes galactic rotation curves also determines why photons are massless ($P = 0 \Rightarrow$ Goldstone theorem), why protons are massive ($P \to 1 \Rightarrow$ topological winding energy), why neutron stars obey GR ($P = 1 \Rightarrow$ perfect screening), and why the universe has dark matter ($P_0 < 1 \Rightarrow \chi_{\rm Avr} = 0.276$).

Several features have no standard analog: (i) a continuous $P$-parameter replacing discrete state categories, (ii) $P$-dependent time flow, (iii) the creative capacity function, (iv) universal phase transition mechanism, and (v) dark matter as a $P$-field state rather than a particle species.

## XI. PREDICTIONS

### A. Conformal anomaly

The trace anomaly coupling predicts a fine structure constant variation:

$$\frac{\Delta\alpha}{\alpha} \sim \frac{|b|}{64\pi^2} \ln \frac{P}{P_0} \sim 10^{-4} \quad \text{at halo edges}\,, \tag{24}$$

where $b = -32/3$ is the SM beta function coefficient. Current QSO constraints reach $\sim 10^{-5}$.

### B. Cluster gravitational redshift

DCT predicts a gravitational redshift 8% deeper than GR for galaxy clusters:

$$\Delta v(\text{DCT}) = -10.8 \text{ km/s} \quad \text{vs observed } -10 \pm 3 \text{ km/s}\,. \tag{25}$$

### C. Splashback radius

$$\frac{R_{\rm sp}(\text{DCT})}{R_{\rm sp}(\Lambda\text{CDM})} = \sqrt{P_0} = 0.923\,, \tag{26}$$

or 7.8% smaller. DES Y3 measures $R_{\rm sp}/R_{200m} = 0.86 \pm 0.05$: DCT is $1.8\sigma$ from data versus $\Lambda$CDM at $3.2\sigma$.

### D. Growth index

$$\gamma(\text{DCT}) = 0.695 \quad \text{vs} \quad \gamma(\text{GR}) = 0.553\,. \tag{27}$$

A 26% difference testable by DESI Y3 (2027) and Euclid (2028). Current $f\sigma_8$ data already favor DCT: $\Delta\chi^2 = 12.5$ over $\Lambda$CDM at 19 redshift bins.

### E. Modified Schwinger pair creation

The $P$-dependent critical field [9]:

$$E_{\rm cr}(\text{DCT}) = P_0 \times E_{\rm cr}(\text{QED}) = 1.126 \times 10^{18} \text{ V/m}\,, \tag{28}$$

predicts pair creation onset 14.9% below the standard QED value. Testable at ELI-NP and SEL by 2030–2035.

### F. BEC analog experiments

The quantum droplet three-body coupling $\beta = g_3/g_2 = 5/3$ is testable in existing laboratories [7]. Four signatures: (i) droplet density 10% above LHY-only, (ii) breathing mode shifted 5%, (iii) critical atom number 40% lower, (iv) three-body loss rate enhanced by factor $25/9 \approx 2.78$.

### G. FRB dispersion measure scatter

The $P$-field viscosity (Re $\sim$ 0.0008) predicts $\sim 15\%$ suppression of FRB DM scatter. Testable with $> 100$ localized FRBs.

### H. Satellite velocity dispersion

$$\frac{\sigma_v(\mathrm{DCT})}{\sigma_v(\Lambda\mathrm{CDM})} = \frac{1}{\sqrt{P_0}} = 1.084\,, \tag{29}$$

an 8.4% boost, consistent with observed 5–10% velocity bias.

## XII. SUMMARY AND CONCLUSION

Dimensional Coherence Theory provides a complete and unified taxonomy of states of matter through the single parameter $P$—the Parrott field condensate order parameter. From photons ($P = 0$) to neutron star surfaces ($P = 1$), from the pre–Big Bang vacuum to galaxy halos, every state of matter corresponds to a configuration of one scalar field governed by one equation.

The key results are: (1) all conventional states correspond to ranges of local $P$; (2) nine condensate configurations span $P \in [0, 1]$; (3) the creative capacity $\mathcal{C}(P) = \sqrt{P}/(1 - P)$ explains why life concentrates at high-$P$ topological defects; (4) the rendering interpretation identifies proper time as the condensate refresh rate; (5) eight testable predictions distinguish this framework from standard physics.

The Parrott field is not merely a classification tool but a physical field with measured consequences: it resolves the Hubble tension ($H_{\mathrm{phys}} = 73.1$ km/s/Mpc), explains dark matter without particles (RAR from Avrami crystallization, 175 galaxies, zero free parameters), and predicts a measurable PPN deviation ($\gamma - 1 = -2.0 \times 10^{-5}$, BepiColombo $6.7\sigma$).

The universe, in DCT, is a superfluid condensate. Every atom, every photon, every black hole is a configuration of that condensate. The diversity of matter is the diversity of one field.

## ACKNOWLEDGMENTS

The author acknowledges the use of Claude (Anthropic) for computational assistance and manuscript preparation. All scientific content, theoretical derivations, and physical interpretations are the sole work of the author.

[1] N. G. Parrott, "Dimensional Coherence Theory: A Brans-Dicke Condensate Unification of Gravity, Quantum Mechanics, and Particle Physics," Paper 0, DCT-2026-001 (2026).

[2] N. G. Parrott, "DCT I: Resolution of the Hubble Tension, $S_8$ Tension, and Growth Rate Anomaly with Zero Free Parameters," Paper I, DCT-2026-002 (2026).

[3] N. G. Parrott, "DCT III: Dark Matter Without Particles—Avrami Crystallization of the Parrott Field and the Radial Acceleration Relation," Paper III, DCT-2026-004 (2026).

[4] N. G. Parrott, "DCT IV: The Standard Model Gauge Group from 600-Cell Topology via the McKay Correspondence," Paper IV, DCT-2026-005 (2026).

[5] N. G. Parrott, "DCT V: Proton-to-Electron Mass Ratio, CKM Mixing, and Baryon Asymmetry from the 600-Cell Spectral Identities," Paper V, DCT-2026-006 (2026).

[6] N. G. Parrott, "DCT VI: The Parrott Bridge—Quantum Mechanics as Phase Dynamics, General Relativity as Amplitude Dynamics, and Their Unification via the Gross-Pitaevskii Equation," Paper VI, DCT-2026-007 (2026).

[7] N. G. Parrott, "DCT VII: BEC Analog Experiments—Quantum Droplet Predictions and Laboratory Tests," Paper VII, DCT-2026-008 (2026).

[8] N. G. Parrott, "DCT VIII: The 600-Cell as Fundamental Spacetime Lattice—Adjacency Spectrum, Spectral Identities, and the $\sqrt{5}$ Cancellation Theorem," Paper VIII, DCT-2026-009 (2026).

[9] N. G. Parrott, "DCT X: Nine Forces of Nature—Complete Force Catalog from a Single Condensate Field," Paper X, DCT-2026-011 (2026).

[10] N. G. Parrott, "DCT XI: Atoms and Elements from the 600-Cell—The Conformal Wall Theorem and 118 Elements," Paper XI, DCT-2026-012 (2026).

[11] S. S. McGaugh, F. Lelli, and J. M. Schombert, "Radial Acceleration Relation in Rotationally Supported Galaxies," Phys. Rev. Lett. **117**, 201101 (2016). doi: 10.1103/PhysRevLett.117.201101; arXiv:1609.05917.

[12] Planck Collaboration (N. Aghanim *et al.*), "Planck 2018 results. VI. Cosmological parameters," Astron. Astrophys. **641**, A6 (2020). doi:10.1051/0004-6361/201833910; arXiv:1807.06209.

[13] A. G. Riess *et al.*, "A Comprehensive Measurement of the Local Value of the Hubble Constant with 1 km s$^{-1}$ Mpc$^{-1}$ Uncertainty from the Hubble Space Telescope and the SH0ES Team," Astrophys. J. Lett. **934**, L7 (2022). doi: 10.3847/2041-8213/ac5c5b; arXiv:2112.04510.

[14] S. More *et al.* (DES Collaboration), "Detection of the Splashback Radius and Halo Assembly Bias of Massive Galaxy Clusters," Astrophys. J. **825**, 39 (2016). doi: 10.3847/0004-637X/825/1/39; arXiv:1601.06063.

[15] B. P. Abbott *et al.* (LIGO Scientific and Virgo Collaborations), "Observation of Gravitational Waves from a Binary Black Hole Merger," Phys. Rev. Lett. **116**, 061102 (2016). doi:10.1103/PhysRevLett.116.061102;

arXiv:1602.03837.

[16] C. R. Cabrera, L. Tanzi, J. Sanz, B. Naylor, P. Thomas, P. Cheiney, and L. Tarruell, "Quantum liquid droplets in a mixture of Bose-Einstein condensates," Science **359**, 301 (2018). doi:10.1126/science.aao5686; arXiv:1708.07806.

[17] L. P. Pitaevskii and S. Stringari, *Bose-Einstein Condensation* (Oxford University Press, Oxford, 2003).

[18] E. P. Gross, "Structure of a quantized vortex in boson systems," Nuovo Cimento **20**, 454 (1961). doi: 10.1007/BF02731494

[19] L. P. Pitaevskii, "Vortex lines in an imperfect Bose gas," Sov. Phys. JETP **13**, 451 (1961).

[20] C. Brans and R. H. Dicke, "Mach's Principle and a Relativistic Theory of Gravitation," Phys. Rev. **124**, 925 (1961). doi:10.1103/PhysRev.124.925

[21] J. D. Bekenstein, "Relation between physical and gravitational geometry," Phys. Rev. D **48**, 3641 (1993). doi: 10.1103/PhysRevD.48.3641; arXiv:gr-qc/9211017.

[22] S. M. Allen and J. W. Cahn, "A microscopic theory for antiphase boundary motion and its application to antiphase domain coarsening," Acta Metall. **27**, 1085 (1979). doi:10.1016/0001-6160(79)90196-2

[23] M. Avrami, "Kinetics of Phase Change. I. General Theory," J. Chem. Phys. **7**, 1103 (1939). doi: 10.1063/1.1750380

[24] J. D. Bekenstein, "Black holes and entropy," Phys. Rev. D **7**, 2333 (1973). doi:10.1103/PhysRevD.7.2333

[25] S. W. Hawking, "Particle creation by black holes," Commun. Math. Phys. **43**, 199 (1975). doi: 10.1007/BF02345020

[26] J. M. Lattimer, "The Nuclear Equation of State and Neutron Star Masses," Annu. Rev. Nucl. Part. Sci. **62**, 485 (2012). doi:10.1146/annurev-nucl-102711-095018; arXiv:1305.3510.

[27] W. Heisenberg and H. Euler, "Folgerungen aus der Diracschen Theorie des Positrons," Z. Phys. **98**, 714 (1936). doi:10.1007/BF01343663

[28] J. Schwinger, "On Gauge Invariance and Vacuum Polarization," Phys. Rev. **82**, 664 (1951). doi: 10.1103/PhysRev.82.664